Fabrication of activated carbon fibers/carbon aerogels composites by gelation and supercritical drying in isopropanol

Ruowen Fu
Massachusetts Institute of Technology, 77 Massachusetts Avenue, Cambridge, Massachusetts 02139, and PCFM Laboratory, Zhongshan University, Guangzhou, 510275 People's Republic of China

Bo Zheng and Jie Liu
Department of Chemistry, Duke University, Durham, North Carolina 27708

Steve Weiss, Jackie Y. Ying, Mildred S. Dresselhaus,[a] and Gene Dresselhaus
Massachusetts Institute of Technology, 77 Massachusetts Avenue, Cambridge, Massachusetts 02139

Joe H. Satcher, Jr. and Theodore F. Baumann
Lawrence Livermore National Laboratory, P.O. Box 808, Livermore, California 94551

(Received 5 April 2003; accepted 5 August 2003)

Activated carbon fiber/carbon aerogel (ACF/CA) composites were fabricated by gelling a mixture of ACF and resorcinol and furfural, followed by supercritical drying of the mixture in isopropanol. The product then went through carbonization in a nitrogen atmosphere. The fabrication conditions, such as the mass content of R–F, the content of the ACF added, and the gelation temperature, were explored. The textures and pore structures of the ACF/CA composites thus obtained were characterized using transmission electron microscopy, scanning electron microscopy, and a surface area analyzer. The mechanical properties of the samples were assessed primarily through compressive tests. The experimental results indicated that the added ACF disperses uniformly in the resulting ACF/CA composites. The carbon matrix of the ACF/CA composites also consisted of interconnected carbon nanoparticles with sizes in the range of 20 to 30 nm. The ACFs can reinforce the related carbon aerogels when they originally have low mass density and are weak in mechanical strength. When large amounts of ACF were added to the composites, the micropore area and micropore volume of the composites increased, but their external surface area decreased. The mesopore volumes and the related diameters and mesopore size distributions of the ACF/CA composites were mainly affected by the mass density of the composites. The micropore sizes of all the composites were sharply concentrated at about 0.5 nm.

I. INTRODUCTION

Generally, carbon aerogels are fabricated through the sol-gel polymerization of resorcinol with formaldehyde in aqueous solution, followed by exchanging with an organic solvent such as acetone, and then exchanging with liquid CO_2 and drying under CO_2 supercritical conditions, and finally carbonizing at elevated temperatures under a N_2 atmosphere.[1] Recently we developed a new fabrication method for carbon aerogels by synthesizing and supercritical drying an organic aerogel in isopropanol. Based on our previous studies,[2] we have found that this polymerization system presents a very rapid cross-linking speed, so that the gelation time is usually several minutes. Around the gel point, it takes only several seconds for the transition of the polymerization system from a liquid into a solid. The rapid consolidation of this new method allows us to synthesize a composite of activated carbon fiber (ACF) and organic aerogel, because the rapid consolidation will prohibit the precipitation and separation of ACFs from the solution.

The fabrication of activated carbon fiber/carbon aerogel composites (ACF/CA) is an interesting subject both for science and technical applications. On the one hand, ACF is a novel material with abundant micropores, whereas carbon aerogels contain large amounts of mesopores and even macropores. Therefore we can design various porous carbon materials with expected pore structures by the design of ACF/CA composites. On

[a] Address all correspondence to this author.
e-mail: millie@mgm.mit.edu

the other hand, typical carbon aerogels have poor mechanical properties, such as low strength and fragility. The reinforcement of CA by ACF is expected to improve its mechanical properties. Up to now, many papers have reported studies of the fabrications, structures, and applications of carbon aerogels.[3–6] Some scientists paid attention to studies of metal/CA composites (metal-doped carbon aerogels).[7–10] J. Wang *et al.* reported the study of carbon cloth–reinforced carbon aerogel films derived from resorcinol formaldehyde.[11] However, there are no literature reports to our knowledge related to the study of ACF/CA composites.

Therefore, the objectives of the present research were to explore: (i) the fabrication of ACF/CA composites by synthesizing and supercritical drying the ACF/CA gel in isopropanol, based on previous studies;[1] (ii) the carbon nanostructures and morphology of the ACF/CA samples obtained by transmission electron microscopy (TEM) and scanning electron microscopy (SEM) observation; and (iii) the pore structure and pore size distribution of the ACF/CA samples by surface area analyzer determination.

II. EXPERIMENTAL

A. Synthesis of ACF/CA composites

ACFs containing organic aerogels were synthesized by the following procedure: dissolving resorcinol and furfural (with molar ratio 1:2) in isopropanol in a vial, adding ACF [activated with steam, Brunauer–Emmett–Teller (BET) area: ~850 m^2/g, diameter: ~10 μ; length: 0.05 to ~0.3 mm] into the solution, heating to 70 to 75 °C in an oil bath, adding 1 vol% hydrochloric acid (37%) as a catalyst, and sealing the vial to polymerize the organic aerogel, while stirring the mixture before the consolidation of the reaction system. After 30 min, the reaction temperature was raised to the aging temperature (75 °C) to react the mixture for 48 to 64 h. The composite gel cylinders thus obtained were transferred into a pressure vessel to dry under isopropanol supercritical conditions (heating from 25 to 265 °C for 3 h, then maintaining at 265 °C for 25 min). The aerogels thus obtained are denoted by ACF/AG.

The resulting ACF/AG cylinders were carbonized within a quartz tube furnace at 800 °C for 3 h under an N_2 atmosphere. These composites were denoted by ACF/CA. The mass densities of ACF/AG and ACF/CA were determined by measuring the dimensions and mass of each sample.

The ACFs were prepared by impregnating rayon fiber precursors with 5% diammonium hydrogen phosphate solution, drying at 110 °C, carbonizing at 900 °C in an inert atmosphere, and then activating at 850 °C with a gas mixture of water vapor and nitrogen in a quartz tube furnace.

B. TEM observations

Some powders were scraped from the resulting bulk samples and dispersed with water onto a copper grid for microscopic examination. The structures of the ACF/CA composites were observed using a JEM 2000FX (JEOL Ltd., Tokyo, Japan) transmission electron microscope.

C. SEM observations

The ACF/CA composites were mounted on a sample holder, coated with Au/Pd alloy, and then observed using a JEM-6320FV (JEOL Ltd., Tokyo, Japan) scanning microscope.

D. Test of the mechanical properties

The carbon aerogel samples were processed into a size of about 22 mm width, 5 mm breadth, and 5 mm height. The maximum (break) compressive force on the samples was detected under uniaxial compression with the accessory shown in Fig. 1, using a H10K-S universal testing machine (Hounsfield Test Equipment Ltd., Salfords, United Kingdom). The compression speed was 1 mm/min.

E. Measurement of the pore parameters and pore size distribution

Samples of approximately 0.1 g were heated to 200 °C to remove all adsorbed species. Nitrogen adsorption isotherms were then taken using an ASAP 2000 surface area analyzer (Micromeritics Instrument Corporation, Norcross, GA). The BET surface areas were calculated by BET theory. The micropore area, micropore volume, and external surface area were calculated by t-plot theory, the median pore diameter and micropore size distribution were analyzed by the Horvath–Kawazoe (HK) theory, micropore theory (MP), and desorption cumulative pore volume, BJH desorption average pore diameter, and mesopore size distributions were analyzed by Barrett–Johner–Halenda theory (BJH),[12] respectively.

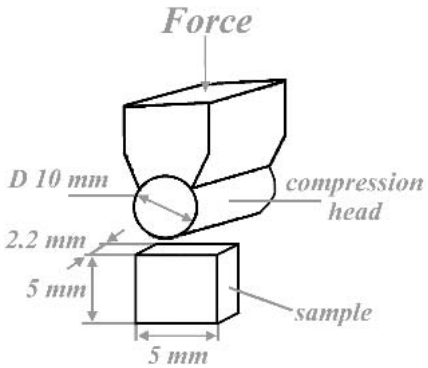

FIG. 1. Schematic diagram of uniaxial compression accessory and method.

III. RESULTS AND DISCUSSION

A. Synthesis of the ACF/CA composites

Based on the basic synthesis recipe of carbon aerogels by gelation and supercritical drying in isopropanol,[2] in the present work we mainly focused on the factors of the mass content of resorcinol–furfural (R–F), the content of ACF used, and the gelation temperature in the synthesis of ACF/CA composites. The fabrication results are listed in Table I. We were able to obtain ACF/CA composites of different densities by mainly controlling the mass content of R–F and the content of added ACF. We found that the effects of the synthetic conditions on the density of the ACF/CA composites are similar to that discussed in the previous report.[2] The comparison of samples FU-64, FU-65, and FU-66 showed that the density of the ACF/AG and of the related ACF/CA composites decreases, accompanying a decrease in the mass content of the R–F precursor. When the amount of ACF used increases, the density of the ACF/AG and of the related ACF/CA composites increases to some extent, from the comparison of samples FU-48, FU-49, and FU-50. The gelation time is not apparently affected by the addition of ACF, but it is prolonged with a decrease of the mass content of R–F because a decrease of the reactants slows down the speed of polymerization as well as the speed of cross-linking. We found that even though the gelation times of the samples listed in Table I are different, the duration times of the transformation of various reaction systems from a liquid into a solidified gel, which is only about several seconds, is not apparently different. For this reason, the dispersion of the ACF in the reaction solution can be maintained as the mixture is quickly solidified, and therefore the ACF maintains a uniform distribution in the composites (which will be further discussed in Sec. III. C).

The higher polymerization temperatures accelerate the polymerization speed and promote the interchain cross-linking, and therefore the gelation time of the reaction system is slightly shortened and the mass density of the ACF/CA is decreased when the gelation temperature rises from 70 to 75 °C. However, we do not suggest the use of a gelation temperature of 75 °C because this temperature is too near the boiling point of isopropanol (82.4 °C). The reaction of resorcinol and furfural generates heat. If we cannot remove the generated heat quickly, the local temperature of the reaction system might rise to higher than the boiling point of isopropanol, which would produce some large holes in the composites. Therefore the synthesis at a 75 °C gelation temperature is very hard to control.

B. TEM observations of the ACF/CA composites

The TEM observation of the carbon nanostructures in the ACF/CA composites is shown in Fig. 2. We can see that the carbon matrix of the ACF/CA composites is also

TABLE I. The effects of synthesis conditions on the density of the ACF/AG and the related ACF/CA.

	FU-48	FU-49	FU-50	FU-64	FU-65	FU-66
Mass content of R–F (%)	16.7	16.7	16.7	16.7	11.5	5.9
Content of ACF (wt.%)	3	5	8	11	16	25
Gelation temperature (°C)	75	75	75	70	70	70
Gelation time (min)	1.8	1.8	1.8	2.0	3.5	6.5
Aging duration (h)	48	48	48	64	64	64
Density of ACF/AG (mg/ml)	319	313	345	402	286	164
Density of ACF/CA (mg/ml)	386	387	423	488	356	187

Catalyst used = 1 vol% HCl; aging temperature = 75 °C; carbonization temperature = 800 °C.

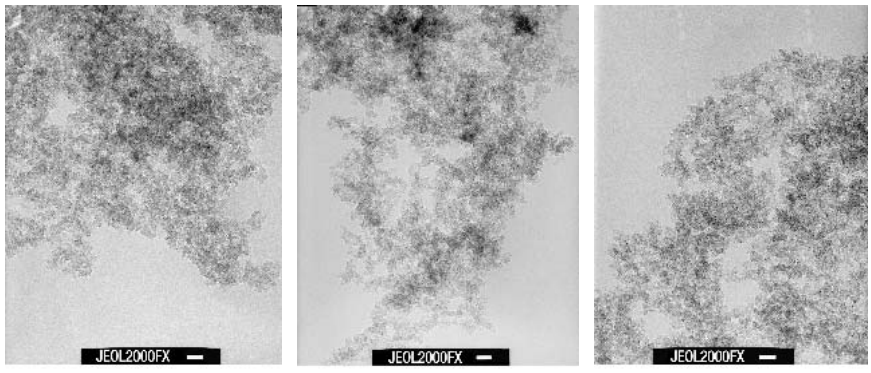

FIG. 2. TEM photographs of the ACF/CA composites: (a) ACF/CA FU-64, (b) ACF/CA FU-65, and (c) ACF/CA FU-66.

composed of interconnected carbon nanoparticles with sizes ranging from 20 to 30 mm, which are almost the same as in the typical carbon areogels reported in the literature.[2,4] When the density of the ACF/CA is changed, the size and the shape of the individual carbon nanoparticles in various composites remain almost the same, but the density of holes in the carbon matrix is increased with a decrease in the mass density of the ACF/CA. These results are the same as in the blank CA (without ACF),[2,13] indicating that the addition of ACF into the reaction system does not affect the carbon nanostructures of the CA matrix.

C. SEM observations of the ACF/CA composites

The SEM observations in Fig. 3 further show the carbon nanostructure of the ACF/CA composites. It can be seen from Fig. 3 that there are abundant mesopores and macropores in the ACF/CA. The number of macropores in the carbon matrix obviously increases with a decrease in the mass density of the ACF/CA, similar to the texture of the CAs reported elsewhere.[4,13]

To assess the dispersion of the ACFs in the CA matrix, we examined the textures of the cylinder-shaped sample FU-65 at the bottom, middle, and top locations, respectively, using SEM. We found that the density of the ACF dispersed at the bottom, middle, or top positions of the sample cylinder are almost identical, as shown in Figs. 4(a), 4(c), and 4(e). (The arrows show the ACF positions.) In most cases, the ACF is individually separated in the CA matrix, whereas very few bundles of ACFs can be observed in the ACF/CA composites, indicating that the ACFs are dispersed quite evenly in the samples. Furthermore, the high-resolution SEM photographs recorded at the bottom, middle, and top position

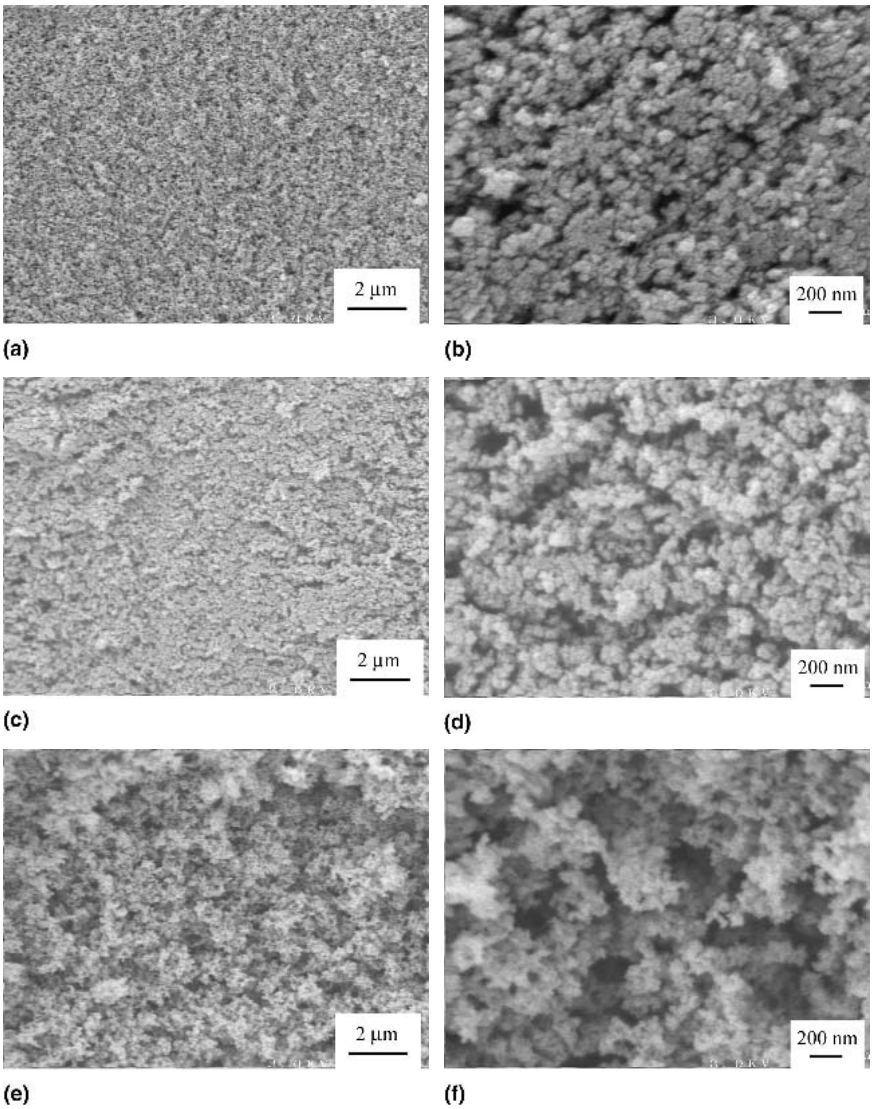

FIG. 3. SEM photographs of the ACF/CA composites with various mass densities: (a) and (b) ACF/CA FU-64, (c) and (d) ACF/CA FU-65, and (e) and (f) ACF/CA FU-66.

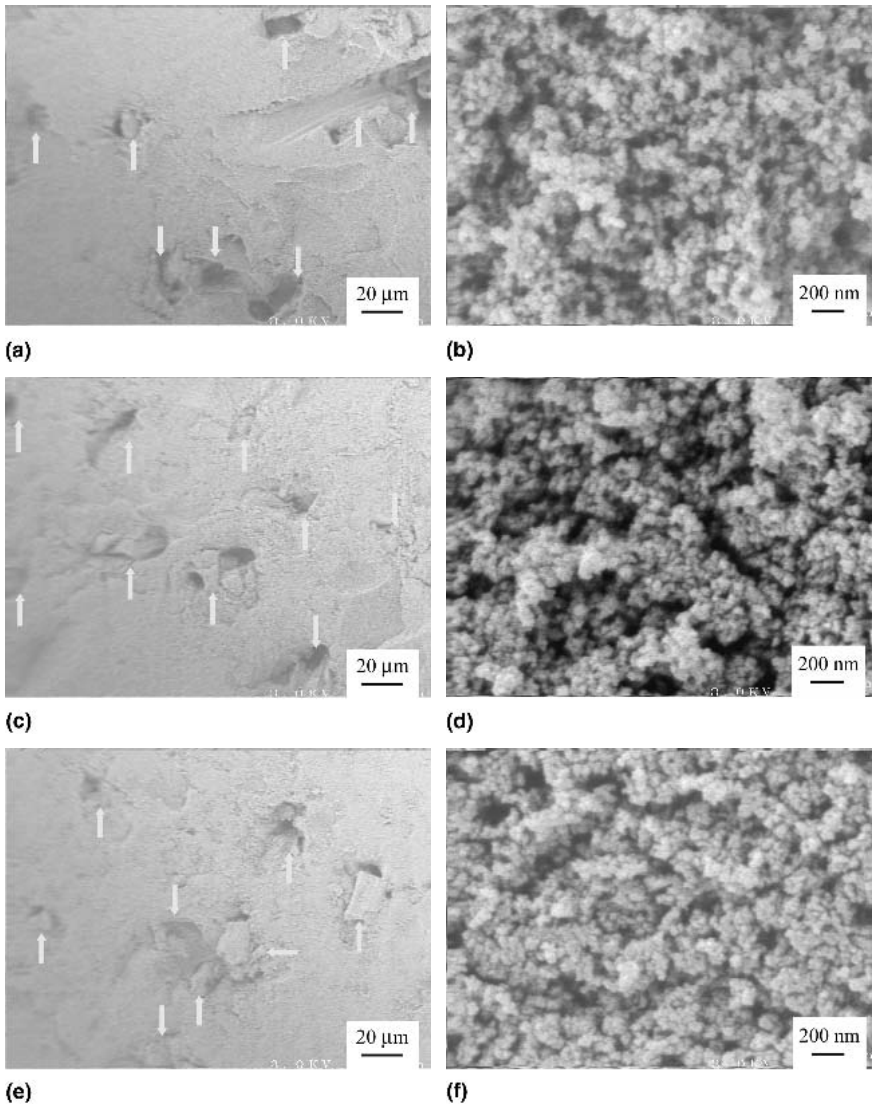

FIG. 4. SEM photographs at different locations of the FU-65 cylinder: (a) and (b) in bottom area, (c) and (d) in middle area, and (e) and (f) in top area.

of the FU-65 sample, as shown in Fig. 4(b), 4(d), and 4(f), show that the size, shape, and packing density of the carbon nanoparticles in the ACF/CA are almost the same everywhere, indicating a uniform texture of the ACF/CA composites.

By observing the interface of ACF and CA using SEM (Fig. 5), we found that the CA particles stick to ACF very well. When the composites are damaged, cracks appear in the carbon matrix, so that some CA particles still remain on the surface of the ACF. This behavior implies that the addition of ACF can improve the mechanical properties of the CA.

D. The mechanical properties of carbon aerogels

Since the CA samples that were prepared were small, we could not prepare standard specimens for tension or flexural tests. Therefore, we designed a uniaxial compression test, shown in Fig. 1, primarily to compare the relative mechanical properties of the ACF/CA and blank CA samples. The compression curves of representative specimens are shown in Fig. 6. The average maximum (break) compressive force values for our samples are summarized in Table II. At the same time, the maximum compressive strength of the specimen was calculated using the compressive force on the cross-sectional area of the specimen, and the results are listed in Table II for comparison. It can be seen from Fig. 6 and Table II that the compressive strength of both the ACF/CA and blank CA series samples decreases with a decrease in the R–F content in gelation (or in their mass density). The more compact the carbon nanoparticles stack, the stronger the aerogel is. After ACFs were added to make an ACF/CA composite, the maximum compressive force (or strength) of the sample is higher than that

of the related blank CA when its R–F content used in gelation (or mass density) is lower than 11.5%. For example, the ACF/CA samples of FU-65 and FU-66, with R–F contents of 11.5% and 5.9%, respectively, have a higher average maximum compressive force and a higher average maximum compressive strength than that of related samples CA-59 and CA-63 (Table II). That is, the ACFs can reinforce the related CAs when the precursor CA has a low density and originally is weak in mechanical strength. However, if the related CAs possess high mass density and thus have a high compressive strength, the addition of ACFs will somewhat decrease the mechanical properties of the samples, since the ACFs themselves are not strong enough.

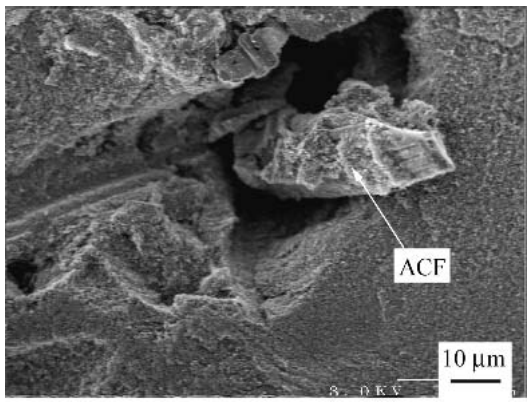

(a)

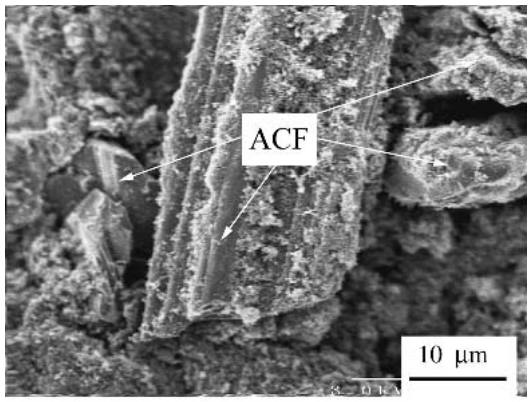

(b)

FIG. 5. SEM photographs of the ACF/CA composites.

E. The surface area and pore structure of the ACF/CA composites

Figures 7 and 8 show the isotherms of the ACF/CA with different ACF contents and various R–F mass contents. All of the isotherms are of the IIb type according to

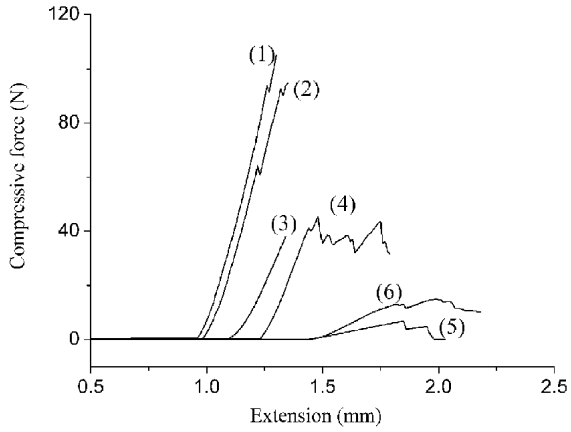

FIG. 6. Compressive force versus extension of carbon aerogels: (1) CA-57, (2) FU-64, (3) CA-59, (4) FU-65, (5) CA-63, and (6) FU-66.

TABLE II. Compressive properties of the ACF/CA composites and related CA samples.

Sample	R–F content (%)	Density of CA (g/cm^3)	ACF content (wt.%)	Test no.	Sample width (mm)	Max. force (N)	Avg. max. force (N)	Max. comp. strength (Mpa)	Avg. max. comp. strength (Mpa)
CA-57	16.7	0.48	0	1	2.27	105	100.7	9.25	9.03
				2	2.18	96.4		8.81	
FU-64	16.7	0.49	11	3	2.26	81.7	93.5	7.20	8.40
				4	2.23	94.7		8.49	
				5	2.12	92.8		8.75	
				6	2.29	104.7		9.14	
CA-59	11.5	0.42	0	7	2.15	32.9	40.0	3.06	3.70
				8	2.22	38.0		3.42	
				9	2.13	49.2		4.62	
FU-65	11.5	0.36	16	10	2.24	46.6	46.0	4.12	4.29
				11	2.07	45.6		4.40	
				12	2.07	56.8		5.49	
				13	2.22	34.8		3.14	
CA-63	5.9	0.15	0	14	2.21	5.17	6.0	0.47	0.56
				15	2.17	6.92		0.64	
FU-66	5.9	0.19	25	16	2.18	15.02	12.3	1.38	1.14
				17	2.18	9.66		0.89	

Sample breadth, 5 mm; sample height, 5 mm.

the International Union for Pure and Applied Chemistry (IUPAC) classification.[11] They are very similar to each other at low and middle relative pressures, while their hysteresis loops are changed under different synthesis conditions. The existence of hysteresis loops indicates that the ACF/CA samples have mesopores. According to these isotherms, the surface area, pore volume, and pore diameter of the ACF/CA composites were analyzed, and the results are listed in Table III. When the mass content remains the same and the amount of ACF used is lower than 10%, the surface areas and the pore volumes of the ACF/CA composites (FU-48, FU-49, and FU-50) are almost the same, indicating that small amounts of the ACF have little effect on the pore structure of the samples. When large amounts of ACF were added into the aerogels, the micropore area and the micropore volume of the ACF/CA composites (FU-64, FU-65, and FU-66) increased. But their external surface area decreased in this case, because the ACF possesses a high surface area and has abundant micropores but not mesopores. Therefore, we can modify the pore structure of CAs to a certain extent by adding ACFs into them. It can be seen from Table III that the BJH desorption cumulative pore volume, the single-point total pore volume, the median pore diameter, the BJH desorption average pore diameter (4V/A), and the average pore diameter (4V/A by BET) all decrease in order from FU-64 to FU-66. This change is mainly related to the decrease of the mass density of the CA matrix, just as discussed in a previous paper.[13]

When the micropore size distribution of the ACF/CA composites was analyzed by the HK theory, it was striking that the micropores of various ACF/CA composites are always sharply concentrated at about 0.5 nm, with a very narrow pore-size distribution (Figs. 9 and 10). We further compared the micropore size distribution of the ACF/CA and related blank CA using the MP theory. It was also astonishing that the micropore size distributions of both the ACF/CA composite and the related CA were the same; that is, the micropores are closely distributed at the radius of 0.25 nm (Fig. 11). CA-62 and CA-63 are the related CAs prepared under the same conditions as

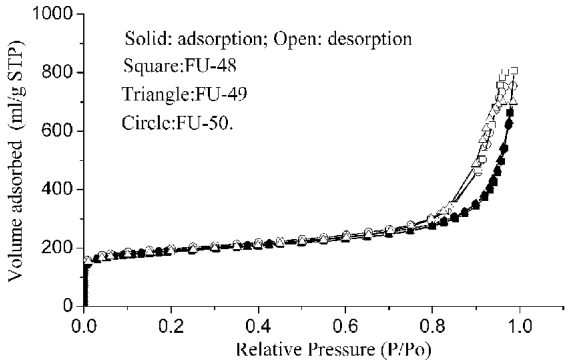

FIG. 7. The adsorption–desorption isotherms of the ACF/CA composites.

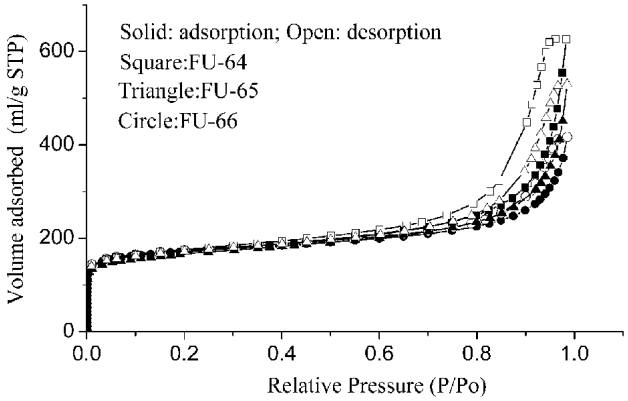

FIG. 8. The adsorption–desorption isotherms of the ACF/CA composites.

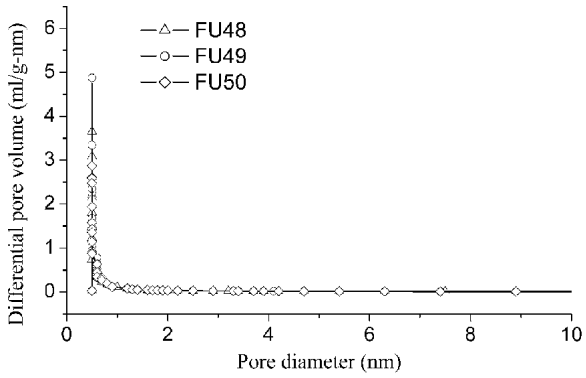

FIG. 9. Micropore distribution of the ACF/CA composites (HK method).

TABLE III. Surface area, pore volume, and pore diameter of the ACF/CA composites.

	FU-48	FU-49	FU-50	FU-64	FU-65	FU-66
BET surface area (m^2/g)	596.2	596.1	616.9	543.6	529.1	540.4
Micropore area (m^2/g)	333.4	335.0	342.2	296.6	303.1	340.2
External surface area (m^2/g)	262.8	261.1	274.7	247.0	226.0	200.2
Micropore volume (ml/g)	0.174	0.175	0.179	0.155	0.158	0.178
BJH desorption cumulative pore volume (ml/g)	1.105	0.935	1.007	0.833	0.669	0.470
Single-point total pore volume (ml/g)	1.249	1.083	1.166	0.969	0.821	0.645
Median pore diameter (nm)	45.64	39.27	36.22	30.30	23.19	8.601
BJH desorption average pore diameter (4V/A) (nm)	14.37	12.32	13.20	11.83	11.16	9.309
Average pore diameter (4V/A by BET) (nm)	8.377	7.266	7.564	7.132	6.204	4.773

FU-65 and FU-66, respectively. These results imply that the micropores coming from the ACF are identical to those coming from the CA matrix. As we know, the micropores in the ACF are produced when the graphite-like layers of the ACF are etched by steam so that some defects remain in the microcrystalline material. We propose that the micropores in the CA are also due to graphite layer defects in the microcrystallites, which are mainly due to the disturbance of cross-linking carbons in the graphite layers of the CA. Intrinsically, the defects are found to be identical in the ACF and in the CA.

The mesopores of the ACF/CA composites also depend on the gaps between the carbon nanoparticles, as has been reported in previous work.[13] When the mass density of the ACF/CA decreases, the gaps between the carbon nanoparticles are enlarged and many of them turn into macropores. Therefore, the mesopore size distributions of the ACF/CA composites are widened and the peak values of the distribution curves are shifted to large diameters with a decrease of the mass density of the composites (Fig. 12). The ACF/CA composites of FU-48, FU-49, and FU-50 were made from the same mass content of R–F and had nearly the same mass density, so that their mesopore size distributions are similar, as shown in Fig. 13.

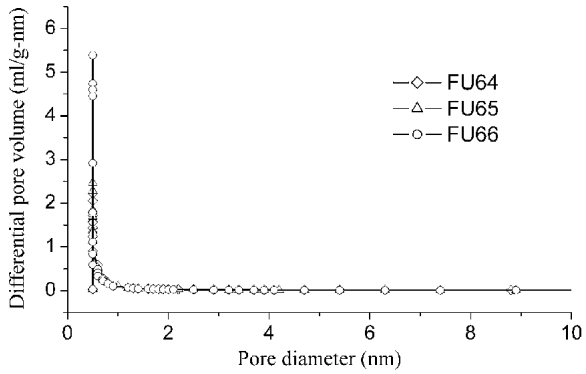

FIG. 10. Micropore distribution of the ACF/CA composites (HK method).

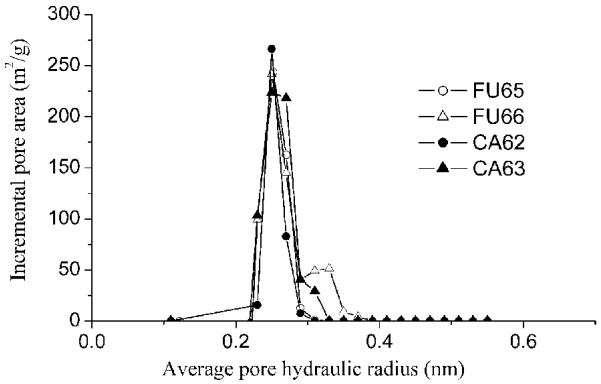

FIG. 11. Micropore distribution of the ACF/CA composites (MP method).

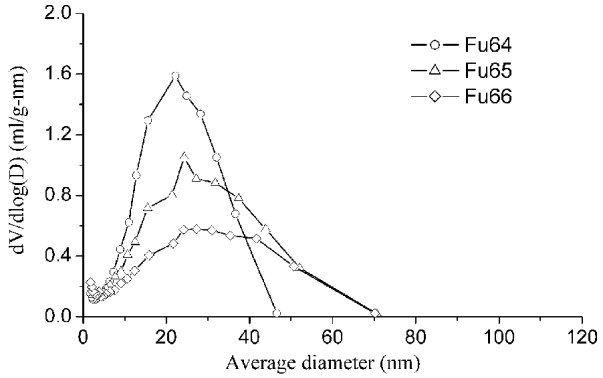

FIG. 12. Mesopore distribution of the ACF/CA composites.

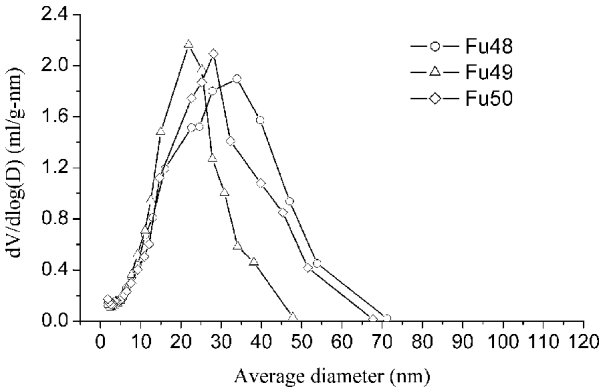

FIG. 13. Mesopore distribution of the ACF/CA composites.

IV. CONCLUSIONS

The ACF/CA composites with a mass density in the range of 180 to 490 mg/ml can be fabricated by polymerizing a mixture of ACF and gel reactants and directly supercritically drying the mixture in isopropanol, then carbonizing the resulting gel in a nitrogen atmosphere. The added ACF is dispersed uniformly in the ACF/CA composites thus obtained. The carbon matrix of the ACF/CA composites is also composed of interconnected carbon nanoparticles with sizes in the range of 20 to 30 nanometers. The ACF does not affect the size and the shape of the individual carbon nanoparticles in the CA matrix. The CA particles in the ACF/CA composite stick to the ACF very well. The addition of ACFs increases the compressive strength of the samples to some extent when they originally have a low mass density and possess weak mechanical properties.

Small amounts of ACF have little effect on the pore structure of the samples, whereas large amounts of ACF increase the micropore area and micropore volume but decrease the external surface area of the ACF/CA composites. The mesopore volumes and the related diameters of the ACF/CA composites decrease and their mesopore size distributions are widened with a decrease in the mass

density of the composites. The micropore size distributions for all of the composites are concentrated at about 0.5 nm. The micropores in the ACF and in the CA are intrinsically identical, though they are formed by different mechanisms.

ACKNOWLEDGMENTS

The research at the Massachusetts Institute of Technology was supported by Lawrence Livermore National Laboratory (LLNL) subcontract B518047 and was partially supported by the Team Project of Guangdong Science Foundation and by the Talents Training Program Foundation of the Higher Education Department of Guangdong Province. Work at Duke University is in part supported by a grant from NASA (NAG-1-01061) through a subcontract from the University of North Carolina.

REFERENCES

1. R.W. Pekala, J. Mater. Sci. **24,** 3221 (1989).
2. R. Fu, B. Zheng, J. Liu, M.S. Dresselhaus, G. Dresselhaus, J.H. Satcher, Jr., and T.F. Baumann, Advanced Functional Materials **13,** 558 (2003).
3. M.S. Dresselhaus, G. Dresselhaus, and P.C. Eklund, *Science of Fullerenes and Carbon Nanotubes* (Academic, New York, 1995).
4. A.W.P. Fung, Z.H. Wang, K. Lu, M.S. Dresselhaus, and R.W. Pekala, J. Mater. Res. **8,** 1875 (1993).
5. R. Desphande, D.M. Smith, and C.J. Brinker, U.S. Patent No. 5 565 142 (1996).
6. R.W. Pekala, C.T. Alviso, X. Lu, J. Gross, and J. Fricke, J. Non-Cryst. Solids **188,** 34 (1995).
7. F.J. Maldonado-Hodar, C. Moreno-Castilla, J. Rivera-Utrilla, Y. Hanzawa, and Y. Yamada, Langmuir **16,** 4367 (2000).
8. J.M. Miller and B. Dunn, Langmuir **15,** 799 (1999).
9. F.J. Maldonado-Hodar, M.A. Ferro-Garcia, J. Rivera-Utrilla, and C. Moreno-Castilla, Carbon **37,** 1199 (1999).
10. T.F. Baumann, G.A. Fox, J.H. Satcher, Jr., N. Yoshizawa, R. Fu, and M.S. Dresselhaus, Langmuir **18,** 7073 (2002).
11. J. Wang, M. Glora, R. Petricevic, R. Saliger, H. Proebstle, and J. Fricke, J. Porous Materials **8,** 159 (2001).
12. F. Rouquerol, J. Rouquerol, and K. Sing, *Adsorption by Powders and Porous Solids, Principles, Methodology and Applications* (Academic, New York, 1999).
13. R. Fu, B. Zheng, J. Liu, S. Weiss, J.Y. Ying, M.S. Dresselhaus, G. Dresselhaus, J.H. Satcher, Jr., and T.F. Baumann, in *The Fabrication of Carbon Aerogels by Synthesizing and Supercritical Drying in Isopropanol,* Program and Short Abstract of Carbon '02, An International Conference on Carbon, p. 140. Proceedings CD-ROM, Sept. 15–19, 2002, Beijing, People's Republic of China.